PNAS
www.pnas.org

Supplementary Information for

Characterizing long-range search behavior in Diptera using complex 3D virtual environments

Pavan K. Kaushik[1*], Marian Renz[2], Shannon B. Olsson[1*]
[1] National Centre for Biological Sciences, Tata Institute of Fundamental Research, Bengaluru, India.
[2] Universität Bielefeld, Bielefeld, Germany.
* Pavan Kumar Kaushik
* Shannon B Olsson
Email: pavan@nice.ncbs.res.in, shannon@nice.ncbs.res.in

This PDF file includes:

SI Appendix
- SI Methods
- Figures S1 to S2
- Tables S1 to S2
- Legends for Movies S1 to S5
- SI References

Other supplementary materials for this manuscript include the following:

- Movies S1 to S5

Supplementary Information

SI Methods

System design

The MultiMoVR engine was written in Python and uses the open source Panda3d game engine (53) for rendering scenes. See (34) for design files and software installation guide for MultiMoVR setup. Diverse virtual Land-Wind-Odorscapes and experimental paradigms can be programmed into the system and added to the Graphical User Interface (GUI) (*SI Appendix*, Fig. S1 A-D) built using pyQtGraph (www.pyqtgraph.org). The virtual environment is designed to provide 3D scenes with precise real time manipulative abilities in all three modalities simultaneously. The virtual world is 1025 m x 1025 m with optional precisely tiled periodic boundaries. The paradigms used in this paper, such as gain optimization, choice assays, plume following, confounding input etc., are already included. Custom scenes can be loaded using .egg or .bam files, which can be designed using Blender (www.blender.org). The system was built on the Robot Operating System (ROS) architecture (54). ROS is used for communication, synchronization and hardware Input-Output. Wing Beat Amplitude Difference (WBAD) is used to close the loop, and was measured in real time from the camera feed using Kinefly (55). To prevent any side bias due to tethering artifacts, a DC offset parameter was adjusted by the user for every tested insect. This made sure that the WBAD distribution was symmetrical. The insect was given a fixed translational velocity (0.5-1 m/s), and based on the insect's virtual position and heading, the Land-Wind-Odorscapes were updated correspondingly in real time.

$$WBAD = LeftWingAmplitude - RightWingAmplitude$$

$$NewHeading = CurrentHeading - Gain * WBAD$$

Dynamic directional airflow and odor was developed and incorporated using a custom-built delivery system (Fig. 1B). The standalone parametric design allows customization to provide "windfields" and odor cues, and an open-source package with a Graphical User Interface (GUI) allows for adjustment of experimental paradigms (*SI Appendix,* Fig. S1B). Dynamic landscapes, windscapes and odorscapes were then created to approximate stimuli that an insect might encounter in the natural world, employing tests that mimicked behaviors observed in the wild for our test species. To close the loop (see definitions in *SI Appendix,* Table S2), we modified a gaming camera to measure wing beat amplitude difference in tethered flying insects and correspondingly adjust the yaw rotation of the scene. As measured directly from input to final closed loop translation visualized on the monitors, the latency of visual, wind and odor components was 66, 36 and 60 ± 4 ms respectively.

A modified PS3 eye camera (Sony Corporation, Japan) was used to film the insect. The camera was chosen for its ultra-low cost, High refresh rate (187 fps) and ease of modification. The IR cut filter was removed to allow observation in IR. A modified C-mount 5 - 50 mm lens (CP-AC550 Pashay, India) with DC iris removed was used in place of the stock lens. However, due to the difference in lens sizes and a constraint to focus very close objects, a custom 3D printed M12 to C-mount extension tube adaptor was attached. The small sensor size along with a large format lens provided magnification, wide focal range and a large working distance at low cost. The camera was mounted on a DSLR macro focus rail (10033981, Neewer, China), which itself is

mounted on a ball head mount (generic). This jointly provides pan, tilt, zoom, x, y and z (focus ring) degrees of freedom for the camera. This allows insects of various sizes (*SI Appendix,* Movie S1, 3), from 2 mm to 40 mm to be filmed with the same setup. Goosenecks from generic USB LED lamps were used for precise fine adjustment of lighting. The dim, visible LED of the gooseneck was replaced with a high power, narrow beam IR emitter (SFH 4550, Osram, Germany). A 3D printed micromanipulator was used for positioning the insect inside the VR.

The wind delivery system design was a result of multiple iterations which tackled issues ranging from unintentional visual input by moving parts, decoupled wind and odor systems, rapid loss of odorant, dramatic loss in air pressure and headspace contamination. The initial design had a simple design of an odor exit port and a suction pipe on a servo arm similar the prior studies. But the motion of the servo itself created unintentional behavioral responses of moving object avoidance by the insects. After multiple attempts at minimizing the visual signature, we resorted to current choice of concealing the moving parts. The next challenge was wind and odor being decoupled. We added 16 capillaries for the wind along with the previous odor exit port. This design allowed the user to control only the direction of the wind but not the direction of odor. This unintentional confounding input produced inconsistent behavioral responses. To remediate this, we connected the odorous line directly into the wind delivery system. This allowed control of both wind and odor direction simultaneously. Initially, there was a severe loss of the air through the bleed holes. But this also meant rapid depletion of odor in the headspace of the odor bottles. Increasing concentrations and volumes did not alleviate this issue as the depletion rate far exceeded the volatility of the blend. To remediate this, we created a U-turn of the odor entering the revolver and exiting only at the aligned hole which reduced odor losses dramatically. Along with this, we added a toroid with precisely placed holes to suck out bleed hole content and local insect headspace and prevent contamination while still having form factor to fit inside the VR and occlude as little of the vision field as possible.

Landscape

The triangular-based prism was composed of three monitors (32 cm X 60 cm). Higher refresh rates to reduce latency, an IPS display with wide viewing angle, and a matte finish are recommended to avoid glare, and thin bezels to minimize edge fixation. The monitor should be able to orient vertically cover a larger solid angle and increase the field of view. For our experiments, an Asus ROG swift, with a 165 Hz IPS panel was chosen, and subtended horizontal field of view of 360° and vertical field of view of 140°. The bezels were 5 mm wide and the luminosity at the insect's location was roughly 1000 lux.

To make the scenery, the tree, for example, was modelled in Blender using 360° photos of fruit trees in an orchard with textures of real fruit, leaves and bark. Seamless textures of grass and clouds were used for the ground and the sky to minimize seam fixation and to add clutter and optic flow. These textures and the virtual lighting were symmetrical to prevent side bias. As the scenery was displayed on flat monitors forming a prism, the scene was corrected for perspective and distortion. The models and textures were scaled, distorted and projected such that they are scaled to real world proportions. So, for example a 3 m tree which is 5 m away subtends the same visual angle for the individual in the VR as it does in the real world (*SI Appendix,* Fig. S1D).

$$RealWorldAngle = 2 * \tan^{-1}\left(\frac{ObjectRadius * \cos\left(2 * \tan^{-1}\left(\frac{ObjectRadius}{ObjectDistance}\right)\right)}{ObjectDistance - \left(ObjectRadius * \sin\left(2 * \tan^{-1}\left(\frac{ObjectRadius}{ObjectDistance}\right)\right)\right)}\right)$$

$$VirtualAngle = 2 * \left(\frac{ObjectRadiusOnDisplay}{DistanceToDisplay}\right)$$

Windscape

The wind delivery system was a custom-built apparatus used to provide airflow and odor from any direction to the insect. There are five main parts to this mechanism. Four static parts with sixteen aligned holes for air to flow, viz., splitter, revolver holder, suction toroid and capillary holder. The revolver is the only moving part with a single hole for air to flow. Filtered, dry air was fed into the splitter at 1 bar. Due to the geometry of the mechanism, only those holes that are aligned with that of the revolver form an unobstructed path for the air to the outlet at the animal. The remaining airflow is shunted through a large concentric bleed hole and removed by the suction toroid. The capillary holder has sixteen L-bent capillaries all pointing radially inward. The individual insect was positioned at the center of these radial spokes, and received airflow depending on which capillary was aligned. The revolver was controlled using a closed loop stepper motor (uStepper NEMA 17, uStepper Aps, Denmark) allowing precise positioning. The revolver alignment hole is 2.5 holes wide (~12.5 mm), and acts as a low pass filter in the transition of the wind direction by smoothing the handoff in the capillary alignments. This was the reason to not choose a valve-based system, as it creates large transients during change in direction and is bulky. Present Mass Flow controllers can provide a smooth handoff but are too slow for our VR. To remediate these artifacts and to cut costs, we resorted to our current design. We used a 3D printer (Raise3D N2, Raise 3D Technologies, USA) to print most of the VR equipment. We used 1.75mm PLA filament (WOL 3D silk, WOL 3D, India), (layer height:0.1mm, nozzle:0.4mm). The 3D designs are resilient and can be replicated with different settings and materials.

The windfield can be loaded as an image mapped to wind direction at that virtual coordinate. The relative angle between the insect's current heading and the wind direction at a virtual location of the insect was used to position the revolver hole. For example, if the insect was heading north and the wind was blowing from the east, the revolver hole was positioned such that the air was blown from the capillary on the right side of the insect. This alignment procedure was performed for every frame in the closed wind condition. In open wind cases, regardless of the insect's heading, the wind always blew from the same front capillary as per the configuration. Image sequences were used for dynamic windfields. Experiment logic using current state was used for context based windfield.

In the slip scenario, the effective translational velocity of the insect was the vector sum of the individual's translational velocity (typically, 0.5 m/s) and wind velocity (typically, 0.2 m/s). Thus, when the insect was heading upwind, its effective translational velocity was 0.3 m/s, while it was 0.8 m/s during downwind heading. But during crosswind and everything between, along with a different velocity, the individual also experienced a visual side slip since the left and right vision fields have different optic flow velocities. All of these parameters can be easily modified in the GUI.

Odorscape

Filtered, dry air at 3 bar was fed into a 3/2 valve. The valve outputs were sent to odor bottles made of PEEK. The odor bottles contained about 400 µl of 10-4 fruit volatile blends made in mineral oil (apple or hawthorn) to provide similar stimulation as prior wind tunnel studies (56) and refilled after about two hours of usage. The control bottles contained only mineral oil. The valve was controlled using a MOSFET relay which received TTL pulses from an Arduino (57). The Arduino sends pulses based on the serial commands sent from the GUI. The output of the odor or control bottles was sent to a hole in the capillary holder. This central hole is aligned with another hole in the revolver creating a non-tangling airflow joint. The air from the revolver passes through a tunnel and exits into the revolver's alignment hole. The upward air current coming from the splitter carries this low velocity valve output. The closed loop stepper motor and the valve receive commands from the GUI and this allows the user to simultaneously simulate mechanical stimulus from any direction and control the timing and duration of odor input with high precision.

The odor field has two layers, odorFrequency and odorLocation. The odorFrequency is a grayscale image, where the brightness corresponds to the packet frequency of the odor. The odorLocation is a binary image, which indicates which coordinates in space have odor and which doesn't. The pixel value of the odorLocation at current virtual position of the individual denotes odor presence/absence. If present, the pixel value of the odorFrequency image at current virtual position denotes the packet frequency of odor. For example, if odorLocation was true and odorFrequency was 3 Hz, then odor was pulsed at 3 puff/second. The puff duration was set to 200 ms, but can be adjusted by the user, to a minimum of 18 ms as per measured system limitations. Using these two images, arbitrary odor plumes can be generated. These images can be drawn by hand using any image editing software and loaded into VR using the GUI.

Although not incorporated in these analyses, odor concentration could also be dynamically altered through the digital flowmeters (Alicat MC-100SCCM-D, USA) at up to 5 Hz.

Speed control

To reduce parameter dimensionality, we maintained constant speed for all experiments. However, to assess specialized behaviors such as potential hovering abilities in VR, we required the additional parameter of speed control when testing the hoverfly, *Eristalis tenax* (*SI Appendix,* Movie S3). We provided speed control by making use of Wing Beat Amplitude Sum (WBAS). The new speed was based on linear transformation of WBAS and this required us to specify four parameters (Min flight speed, Max flight speed, Minimum of WBAS, Maximum of WBAS). This approximation ignores nonlinear effects.

$$WBAS = LeftWingAmplitude + RightWingAmplitude$$

$$NewSpeed = \frac{(MaxSpeed - MinSpeed) * (WBAS - MinWBAS)}{MaxWBAS - MinWBAS}$$

VR initialization

The VR has a virtual area spread across 1025 m x 1025 m. By precise tiling of the textures, the boundaries are setup to have periodic boundary conditions allowing an "infinite" world. Heading is defined as angle with respect to North, which is aligned to the

Y-axis. The insect had an initial virtual location at (513, 513, 1) and 0° heading unless stated otherwise. The product of WBAD and gain was used to move the visual scenery and close the loop. The insect had its translational velocity set to 1 m/s. Once the insect was flying (beating its wings) in the VR, the run was manually initiated. The run was stopped either when the insect stopped flying or when the trajectories overlapped to a reasonable extent, typically after 10 runs. The trial was complete when the reset criterion is met; i.e. when the trial duration exceeded the maximum bout duration parameter, typically 30 s. When the reset event occurred, the individual was virtually teleported back to the same initial position in a new world. The sudden change in visual scenery made insects fling their legs and this resulted in wing tracking errors. To prevent these teleportation artifacts, after every reset, for 0.5 s the insect was in open loop with zero velocity. The next 0.5 s, the insect was in closed loop but still with zero velocity. This allowed the insect to fixate on its object of interest and prevented random initialization artifacts. Only then, the insect's translation velocity was set back to 1 m/s and this entire process repeated after the next reset event. Based on the assay and experiment configuration, there were multiple scene choices to be tested. For example, in the tree assay, there were four parallel worlds: no tree, tree on left, tree on right and trees on both sides. Identical in every aspect except for presence and location of the tree. After every trial reset, the individual was transported to a random selection from one of the 4 worlds to the same start location and orientation, keeping the background and sky scenery identical across the worlds. After teleportation, VR initialization was performed as described before starting the next trial.

Optimal gain determination

We used the optomotor reflex paradigm to measure each fly's compensation to externally imposed yaw rotations. An external turn was imposed on the insect and the insect reflexively compensated for these turns. The turns were repeated clockwise and counterclockwise for a given angular velocity. The angular velocities of these turns were increased exponentially and repeated again in decreasing order. Translational movement was disabled and the insect was only allowed yaw compensation. This entire protocol was repeated on the same individual again with a different gain. Thus, each insect was tested for all achievable combinations of impose velocities and gain. Response was then calculated as the product of the WBAD and gain. Error is defined as the difference between external impose velocity and response of the insect. Stability and maneuverability are for the purpose of this study defined as the mean and s.d. of compensation respectively. Optimal closed loop gain was estimated by measuring the range of gain where stability and maneuverability of the insect's virtual heading to externally imposed yaw rotations were comparable such that if their ratios are close to one, (*SI Appendix,* Fig. S1 E-I)

Insect rearing and preparation

Rhagoletis pomonella (apple fly) were collected and maintained as previously described (56). Briefly, Adult hawthorn and apple race flies were reared from collections of larval-infested fruit sampled at a field site USA using standard *Rhagoletis* husbandry methods and maintained on a 15 L: 9 D light cycle at 22-25 °C and 65% humidity (4). All experiments were performed on sexually mature (12+ days post eclosion) wild Rhagoletis pomonella of both races. The larvae were hand collected from multiple sites in the USA.

Aedes aegypti (Yellow fever mosquito) were obtained as adults from Subaharan Kesavan, NBAIR, Bengaluru, India. *Eristalis tenax* (Hoverfly) were obtained as pupae from Polyfly, Almería, Spain. *Daphnis nerii* (Oleander hawkmoth) larvae were wild caught and reared in greenhouse, NCBS, Bengaluru, India. Wild *Pselliophora laeta* (Crane fly) adults were caught and used for experiments. Insects were maintained in a 23 °C chamber, 60-75% RH in a 14 L-10 D cycle. *R. pomonella* were fed on the artificial diet of sugar and yeast (56), *A. aegypti* on raisins, *E. tenax* on pollen, *D. nerii* on nerium leaves and *P. laeta* on sugar water.

R. pomonella aged between 12 to 20 days post eclosion, *A. aegypti* and *E. tenax* at least 4 days post eclosion were selected that exhibited flight activity in the cage with undamaged wings. Tethered experiments were performed from 1000 to 1800 hrs. at room temperature 22-25 °C (56). *D. nerii* were tested between 1900 and 0100. The insects were cooled in ice for 3 minutes (10 minutes for the hawkmoth) and placed on a cold metal block. A minutien pin glued to a syringe needle was used as the tether. To make identical tethers, a custom jig was built. A tether coated with a tiny drop of cyanoacrylate glue (Fevikwik, Pidilite, India) was lowered and carefully positioned between the insect's head and thorax using a micromanipulator (Narishige, Japan). Using a beard hair, a tiny amount of glue was teased between the gap and allowed to dry for about a minute. The insects were allowed to recover for about 20 minutes in a tiny humidified tip box. A Styrofoam ball (~2mm OD, generic) dipped in sugar solution was given to the insect to provide nutrition and prevent dehydration. Insects that flew on the tether for over 3 minutes were tested in the VR arena. Insects that did not fixate on any target were discarded. For the vision and wind assays, we used head fixed insects, while we used head free insects for odor assays as head fixed insects did not consistently respond to odor. This suggests head movements might be critical for odor tracking.

Software

The front-end GUI of VR was built using Python and pyQtGraph. It can control all the parameters of the VR. Saving and restoring of different default configurations has been added for experimenter's convenience. The live mode section provides real time visualization of trajectories, headings, experimental state variables and live histograms of WBAD. The GUI can also be customized by the user.

The backend of VR was built on top of ROS. The ROS node graph has four major nodes. The camera node preprocesses and publishes the live stream of the camera. The kinefly analyses the live stream and publishes the wing beat angles. The VR node uses the WBAD from kinefly, computes the trajectory and stimulus states and publishes the trajectory. The GUI node subscribes to the trajectory to provide real time visualization. During recording, the trajectory node is subscribed and saved as a rosbag file. This allows for the entire experiment to be replayed, as it is, later for analysis.

To adjust to large graphical and computational loads, we used a gaming PC. It has an i7 5690K CPU (Intel Corporation, USA) and an NVIDIA 980 TI (Nvidia Corporation, USA) GPU with 32 GB RAM running Ubuntu 14.04. The data analysis and statistics was performed on the same computer using custom Python scripts.

Fig. S1. MultiMoVR virtual reality system parameters and calibration.

A photorealistic scene based on real world scenery wrapped around the 3 monitors. (B) Graphical User Interface (GUI) to adjust experiment parameters. (C) Representative optomotor response to a sweep of impose velocities and directions. (D) Perspective calibration. Expected Real World (RW) angles vs measured VR angles of objects. The dashed green line is the reference 45° line. (E) Compensation is defined as the difference between external impose and response by insect. Stability is defined as the mean of compensation, and maneuverability is defined as the s.d. of the compensation. 95% CI indicated as shaded region around lines. Accordingly, gain was set at 75 deg/deg/s (N = 6) for mosquito, (F) 40 deg/deg/s (N = 6) for male crane fly for all subsequent experiments. (G) Female crane fly and (H) Hawkmoth showed no clear optomotor response.

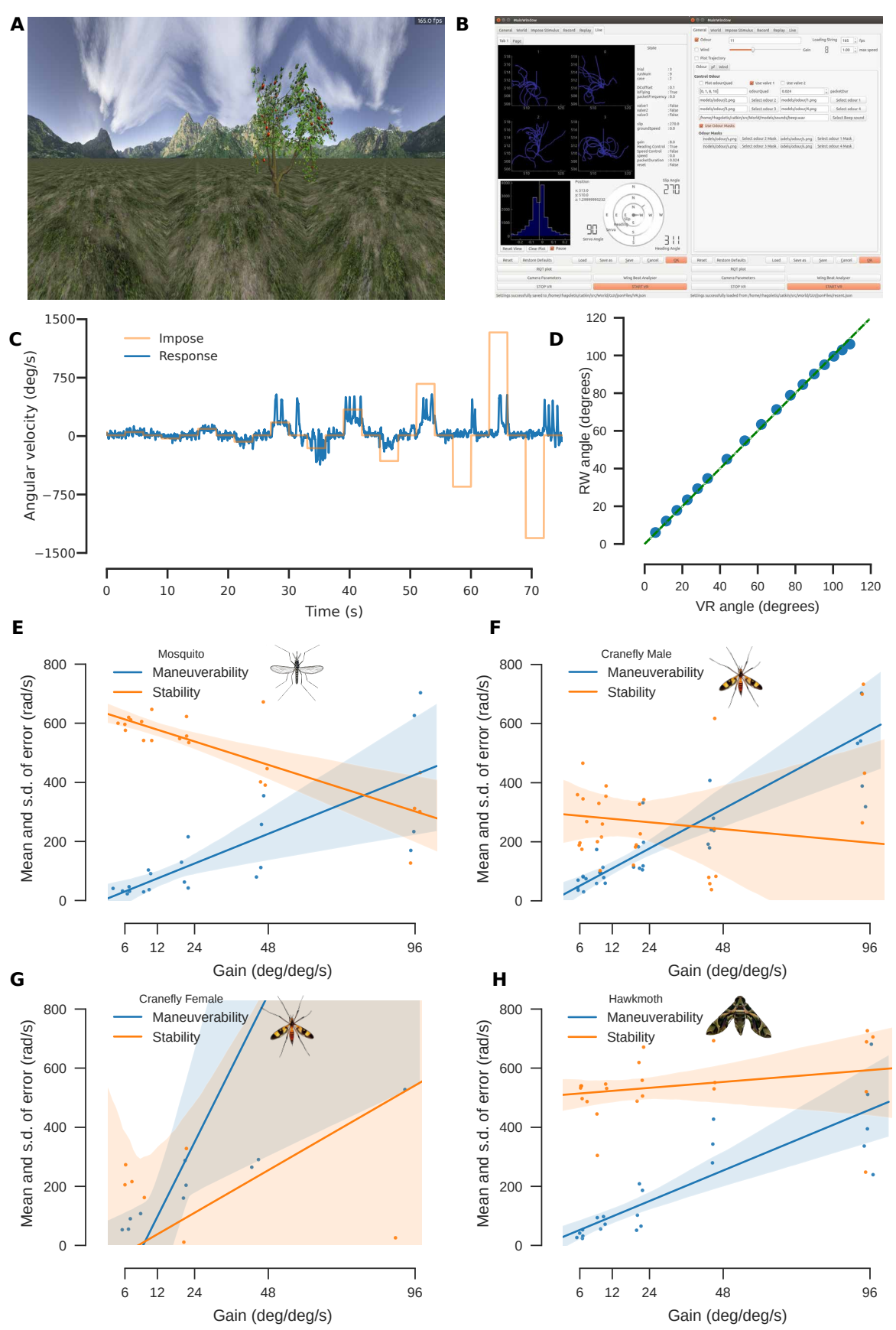
A
165.0 fps
B
C
Impose
Response
Angular velocity (deg/s)
1500
750
0
−750
−1500
0
10
20
30
40
50
60
70
Time (s)
D
RW angle (degrees)
VR angle (degrees)
0
20
40
60
80
100
120
E
Mosquito
Maneuverability
Stability
Mean and s.d. of error (rad/s)
800
600
400
200
0
6
12
24
48
96
Gain (deg/deg/s)
F
Cranefly Male
Maneuverability
Stability
Mean and s.d. of error (rad/s)
Gain (deg/deg/s)
G
Cranefly Female
Maneuverability
Stability
Mean and s.d. of error (rad/s)
Gain (deg/deg/s)
H
Hawkmoth
Maneuverability
Stability
Mean and s.d. of error (rad/s)
Gain (deg/deg/s)

Fig. S2. Raw trajectories in the presence of visual objects.

(A) Two identical 3D models placed side-by-side and viewed equidistantly from the center. Due to parallax, perspective, point of view and structural complexity, the two trees look different from each other. (B) Virtual trajectories of apple fly to worlds with tree on left and (C) tree on both sides, at 3 m virtual distance (N = 11 flies, n = 103 trials). Polar plots representing corresponding mean angles for each trajectory. (D) Virtual trajectories of crane fly to worlds with no tree, (E) tree on left and (F) tree on both sides, at 3 m virtual distance (N = 6 flies, n = 15 trials). (G) Virtual trajectories of mosquito to worlds with no tree, (H) tree on left and (I) tree on both sides, at 3 m virtual distance (N = 6 flies, n = 13 trials). (J) Virtual trajectories of hoverfly to worlds with no flower, (K) flower on left and (L) flower on both sides, at 1 m virtual distance (N = 2 flies, n = 6 trials). (M) Virtual trajectories of apple fly for trees placed at 3, 6, 12 and 24m from initial position (N=20 flies, n=129 trials). (N) Distinguishing distance and size using motion parallax. Raw trajectories of apple fly to large distant trees vs small nearby trees, which subtend identical visual angles at the starting position. (N = 9 flies, n = 96 trials). (O) Virtual trajectories of apple fly in zero optic flow and different directional airflow velocities, 0 m/s, 1 m/s, 2 m/s, 3 m/s (N=22 flies, n=158 trials). (P) Raw trajectories of apple fly for visual slip, slip + odor, slip + windfield, and slip + windfield + odor (N = 8 flies, n = 33 trials). Pink gradient represents odorfield.

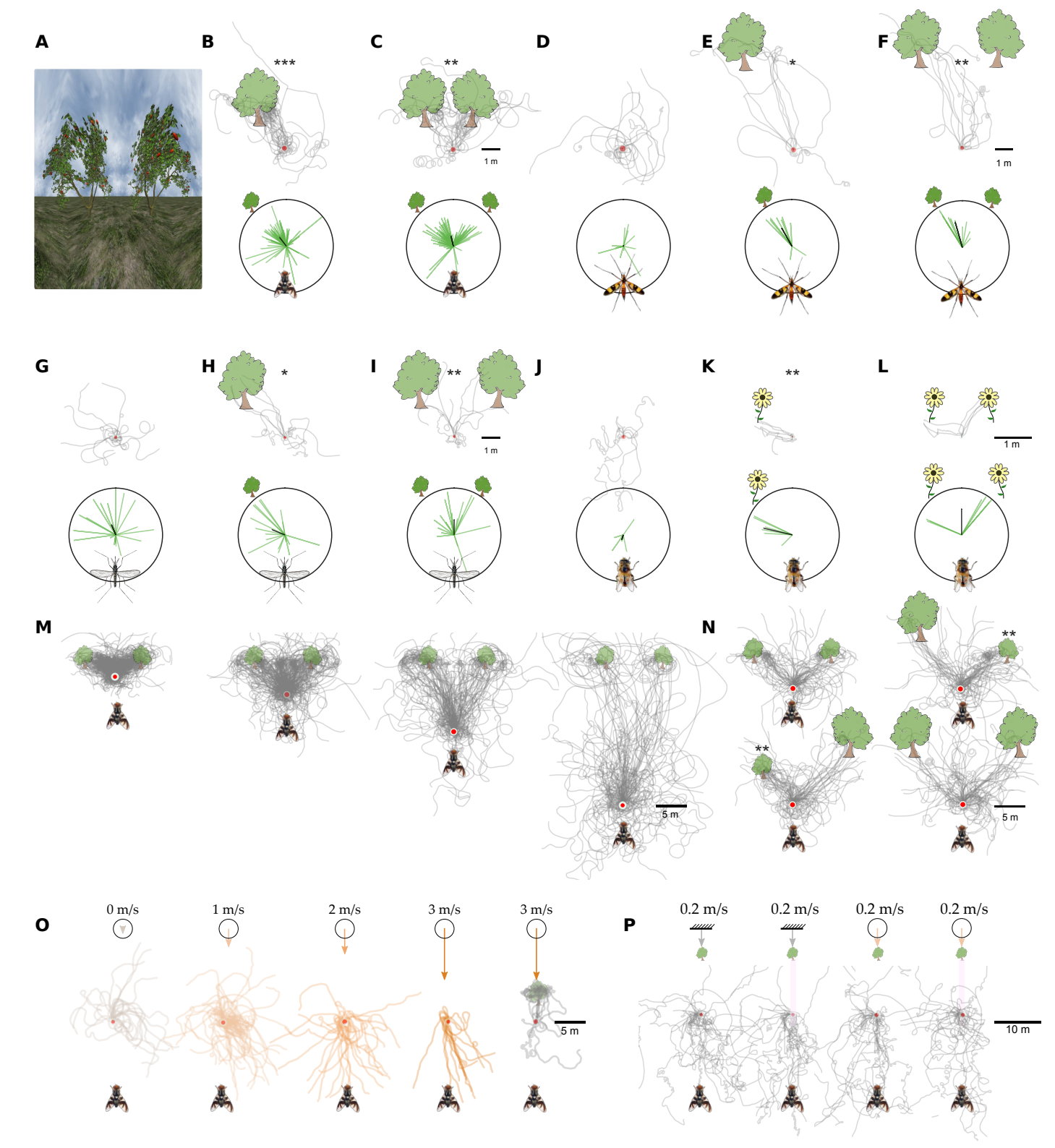
A
B
C
D
E
F
G
H
I
J
K
L
M
N
O
P
***
**
*
1 m
5 m
10 m
0 m/s
1 m/s
2 m/s
3 m/s
3 m/s
0.2 m/s
0.2 m/s
0.2 m/s
0.2 m/s

Table S1. Glossary of VR terms

Keywords	Brief description
Closed loop	Traditional stimulus response experiments are challenging for flying insects due to their size and speed. Tethering allows one to precisely control input and measure the animal's output. But tethering leads to lack of sensory feedback of the animal's motor commands. For example, when a fly intends to turn right, it increases its left wing amplitude more than the right wing creating a rightward yaw torque. In the tethered condition, the fly's motor command will not have any effect on its visual system of being turned right (also known as open loop). By monitoring the fly's wing movements in real time and correspondingly moving the visual scenery, the fly's "intentions" are reflected back on its visual input, known as closed loop.
Virtual Reality	Continuous closed loop feedback of animal's output into its input using artificial visual cues such as image patterns on a drum, projectors, LED panels and monitor displays is what is called VR. This VR concept has extended from being vision-only to include sound, touch, taste etc.
Gain	In closed loop studies, one unit of motion of the insect corresponds to some units of motion in the virtual world, derived from electrical systems as “gain”. At increased gain values, even small motions of the insect creates a large change in the virtual world and vice versa.
Optic flow	Relative motion between an animal and its environment cause visual scenes to move across different regions of its vision field at different velocities. These subtle differences in velocities give organisms, insights of their self-generated movement as well as absolute and relative size and position of objects in the 3D space from a sequence of 2D images on the retina.
Motion parallax	Insects use differences in visual cues and optic flow of landmarks, horizon, angular size and other visual characteristics over time to compute expansion rates of objects in the scenery. This provides the animal with relevant cues of relative position and absolute size of objects critical of navigation and survival.
Slip	When organisms fly in windy environments, the direction of "intended" flight or heading doesn't match the actual motion of the organism. This slight mismatch in heading and in translation direction is due to the wind dragging the organism. There is a lateral asymmetry in the optic flow, which is a function of scenery, wind speed and heading with respect to wind. Insects are known to use these slip cues to orient in the wind while flying.
Odor plumes	Odor plumes are dispersed into the air and broken into tiny packets by turbulent air. These intermittent packets drift along with the meandering wind.
Optomotor anemotaxis	Optomotor anemotaxis is upwind flight by insects guided by the wind direction and visual feedback. Insects compute their direction of motion using optic flow, motion parallax, slip and mechanical cues. These are mostly upwind flights triggered on exposure to odor plumes.

Table S2. Bill of materials

S/L no	Item	Description	Quantity	Rate (USD)	Cost (USD)
1	2020 aluminum frame	Generic extrusions	12 m	5.6	67
2	T-Profile nuts, corner brackets	Generic extrusion attachments	30	0.7	21
3	XY plane DSLR macro slider	Neewer pro 4-way macro focus rail 10033981	1	28	28
4	Ball socket DSLR tripod head	Generic swivel head	1	4	4
5	Web camera with IR hack	Sony PS3 eye, hacked for IR pass and allow C-mount	1	4	4
6	Varifocal C-mount Lens	Pashay CP550 5-50mm C mount lens	1	21	21
7	Closed loop stepper motor	uStepper NEMA 17	1	70	70
8	Arduino microcontroller	Arduino Uno	1	4	4
9	MOSFET relay	Generic IRF540 module	1	1	1
10	High speed 3/2 solenoid valve	Landefeld M3M5 ES 24 V	1	140	140
11	Custom odor bottle	PEEK custom CNC milled	2	28	56
12	Tubing connectors and accessories	Generic T,Y and elbow push fit connectors	20	0.7	14
13	3D printed parts	Wind delivery system, lens holders, manipulators	20 h	2	40
14	IR emitter	SFH 4550, Osram	2	1	2
Sub Total					473
Optional Computer accessories based on reported system					
S/L no	Item	Description	Quantity	Rate (USD)	Cost (USD)
14	Gaming monitors	ASUS ROG Swift PG279q	3	1050	3149
15	CPU	Intel Core i7-5820K Haswell-E 6-Core	1	448	448
16	Motherboard	Asus X99 Sabertooth	1	448	448
17	GPU	Asus Geforce GTX 980 Ti	1	910	910
18	RAM	G.SKILL 32GB (8GB X 4) DDR4	1	224	224
19	SMPS	Antec VP700EC SMPS	1	98	98
20	SSD	Samsung 850 Pro 512GB	2	448	896
21	HDD	Seagate HDD 4 TB desktop	1	154	154

22	Chassis	Cooler Master 690 chassis	1	168	168
Sub Total					6495

Movie S1 (separate file). MultiMoVR arena live overview showing active components with an apple fly controlling the world.

Movie S2 (separate file). Apple fly flying towards a tree-like object with overlays for trajectories and fly wingbeat view.

Movie S3 (separate file). Examples of a mosquito, Aedes aegypti, and a crane fly, *Pselliophora laeta* flying to virtual tree-like objects and a hoverfly *Eristalis tenax*, flying to a virtual flower like object. The hoverfly was also provided with speed control to allow for hovering as shown in the final 10 s of video footage.

Movie S4 (separate file). Example of motion parallax as seen in MultiMoVR with different expansion rates due to differences in the distances to objects.

Movie S5 (separate file**).** Example of an apple fly responding to an odorfield in VR with virtual odor tracking.

SI References

53. M. Goslin, M. R. Mine, The Panda3D graphics engine. *Computer* **37**, 112–114 (2004).

54. M. Quigley, *et al.*, ROS: an open-source Robot Operating System in *ICRA Workshop on Open Source Software*, (Kobe, Japan, 2009), p. 5.

55. G. Maimon, A. D. Straw, M. H. Dickinson, Active flight increases the gain of visual motion processing in Drosophila. *Nat. Neurosci.* **13**, 393–399 (2010).

56. C. Tait, S. Batra, S. S. Ramaswamy, J. L. Feder, S. B. Olsson, Sensory specificity and speciation: a potential neuronal pathway for host fruit odour discrimination in Rhagoletis pomonella. *Proc. Biol. Sci.* **283** (2016).

57. A. D'Ausilio, Arduino: a low-cost multipurpose lab equipment. *Behav. Res. Methods* **44**, 305–313 (2012).